The radio structure of the supernova remnant G315.4-2.3 (MSH14-63)

Dickel, H.R.; Strom, R.G.; Milne, A.B.

DOI
10.1086/318259
Publication date
2001

Published in
Astrophysical Journal

THE ASTROPHYSICAL JOURNAL, 546:447–454, 2001 January 1

THE RADIO STRUCTURE OF THE SUPERNOVA REMNANT G315.4−2.3 (MSH 14−63)

JOHN R. DICKEL[1]
Astronomy Department, University of Illinois at Urbana-Champaign, Urbana, IL 61801
RICHARD G. STROM[2]
ASTRON, 7990AA Dwingeloo, The Netherlands
AND
D. K. MILNE[3]
Australia Telescope National Facility, Epping NSW 1710, Australia
Received 2000 June 13; accepted 2000 August 2

ABSTRACT

G315.4−2.3 is an extended-shell supernova remnant (SNR) with some characteristics of evolutionarily young remnants and some of older ones. To further elucidate some of its characteristics, we present imaging and polarimetry of this SNR at a frequency of 1.34 GHz with a resolution of 8″ made with the Australia Telescope Compact Array. The indicators of youth are as follows: (1) morphologically, the radio emission arises in a smooth shell without the fine-scale filaments seen in the optical; (2) many of the optical filaments are Balmer dominated; (3) where measurable, the orientation of the magnetic field appears to be radial with respect to the center of the remnant; and (4) there may have been a supernova in that region in AD 185. Indications of older age include the following: (1) particularly in RCW 86, the bright optical nebula in the southwestern corner of this extended SNR, but also in other locations there are several filaments with bright [S II] emission representative of older shocked filaments in radiative equilibrium and (2) if the remnant lies at the kinematical distance of 2.8 kpc, it has a diameter of 37 pc which would be large for a remnant less than 2000 years old. The remnant seems to be expanding inside a cavity outlined by infrared emission, and so it could well be young and large. Where it is encountering the walls of the cavity it is slowing rapidly, and we observe the radiative filaments. RCW 86 itself is encountering a dense clump of material but may also be the remains of a more compact lump of ejecta ploughing into the surroundings.

Subject headings: polarization — radiation mechanisms: nonthermal — radio continuum: ISM — supernova remnants

1. INTRODUCTION

The object G315.4−2.3 was first cataloged as the radio source MSH 14−63 by Mills, Slee, & Hill (1961). It was soon recognized as a supernova remnant (SNR) because of its large angular size—about 45′ in diameter—shell structure, radio polarization, and nonthermal radio spectrum (Hill 1967). The bright nebula RCW 86 (Rodgers, Campbell, & Whiteoak 1959) lies in the southwestern corner of the remnant and shows strong [S II] emission, characteristic of shock-excited radiative filaments (Westerlund & Mathewson 1966; Leibowitz & Danziger 1983). Of great surprise, however, was the discovery of faint, very thin Balmer-dominated filaments around almost the entire periphery of the SNR (Long & Blair 1990; Smith 1997). Such features have been recognized in only a small number of SNRs, and they are interpreted as nonradiative ionization of partially neutral hydrogen clouds by passage of the supernova shock, with subsequent recombination to produce the hydrogen emission lines (Chevalier, Kirshner, & Raymond 1980).

There has been considerable discussion as to whether G315.4−2.3 might be the remnant of the supernova of A.D. 185. Arguments in favor include the Balmer-dominated filaments and reasonable positional agreement according to the analysis of historical texts (Clark & Stephenson 1977); arguments against include the large size—a diameter of about 37 pc if it lies at the apparent dynamical distance of 2.8 kpc (Rosado et al. 1996)—and the possibility that the object observed in A.D. 185 may not have been a supernova at all (Chin & Huang 1994; Schaefer 1995). These arguments were summarized by Smith (1997), who notes that the distance and whether the SN was of Type Ia or II (if it was an SN at all) are the crucial points of contention.

Improved radio properties of this SNR, such as a search for fine-scale features, the detailed magnetic field configuration, and the exact relation between radio, optical, and X-ray features, can add more information to this discussion. Both the current radio (Whiteoak & Green 1996) and X-ray (Pisarski, Helfand, & Kahn 1984; Vink, Kaastra, & Bleeker 1997) images show the same general shell seen in Hα and bright emission from RCW 86, but the radio structure of RCW 86 does not match well with the different frequency bands. It has also not been possible to establish any detailed correspondence of specific individual features with the limited 45″ resolution of the best radio image available from the Molonglo Observatory Synthesis Telescope (MOST; Whiteoak & Green 1996). We have therefore observed G315.4−2.3 with the Australia Telescope Compact Array (ATCA; Australia Telescope 1992) with a half-power beamwidth of 8″ at a wavelength of 22 cm to provide higher resolution for both imaging and polarimetry, which previously had only 4′.4 resolution (Milne & Dickel 1974). The equipment and observations will be described in § 2; the results will be presented in § 3; the discussion in § 4 will show that this SNR continues to show several unusual properties; and concluding remarks are in § 5.

[1] Visiting astronomer at ASTRON, 7990AA Dwingeloo, The Netherlands; johnd@astro.uiuc.edu.
[2] Also at Astronomical Institute, University of Amsterdam, The Netherlands; strom@astron.nl.
[3] dmilne@atnf.csiro.au.

2. EQUIPMENT AND OBSERVATIONS

G315.4−2.3 has such a large angular extent that full coverage of the SNR required a 19 point hexagonal mosaic observation, with points spaced slightly less than one-half the primary beamwidth apart. Five configurations of the ATCA were utilized with a total of 70 independent baselines covering a range of spacings between 31 and 6000 m. We note that much of the overall emission of the SNR is still missing, however. The observations recover an integrated flux density of approximately 28 Jy, about 70% of the expected flux density at this frequency (interpolated from the data of Caswell, Clark, & Crawford 1975; Green 1998[4]). The instrument records the intermediate- and fine-scale structure for comparison with the features seen at the other wavelengths but does not show the full brightness of the overall shell.

The many pointing shifts during the mosaicking observations caused high sidelobes with a significant radial spoke pattern. These can be seen around a number of point sources, and one small-diameter double source was present in the region of G315.4−2.3. In particular, the strong source with a flux density of 280 mJy inside the remnant toward the southwest at $\alpha = 14^{h}41^{m}44^{s}.48$ and $\delta = -62°34'47''.1$ (all positions are given for epoch J2000) limited the dynamic range on the image. Phase self-calibration was done on this source for the field centered closest to it, and the results were then transferred to the other pointings with limited success. At the position of RCW 86, about 8′ from the point source, we were able to achieve a dynamic range of about 500/1, which left some ripples in the image at a level of about 0.6 mJy beam^{-1}. For the five 12 hour observations of the 19 point mosaic pattern, the theoretical rms noise level per position should have been about 0.03 mJy. The ripples can be seen cosmetically in the image but do not affect the scientific results. At the angular distance of the east rim, residual effects appear to be less than 0.1 mJy beam^{-1}, the approximate rms noise on the final map or about 3 times the theoretical limit from pure receiver noise. Because the mosaic pattern was large enough to extend well beyond the SNR, the noise is nearly uniform over the whole region shown.

To avoid phase smearing in the outer regions of the beams and also to evaluate the Faraday rotation of the polarized emission by utilizing measurements across the band, the observations were made with a total of 64 channels each 4 MHz wide in two adjacent intermediate frequency (IF) bands. After editing of interference and removal of end channels, a total of 48 channels with a mean frequency of 1389 MHz were used for the final image. For the polarization analysis the data were binned by eight channels into six bands with a width of 32 MHz each between 1310 and 1470 MHz. The six individual 32 MHz bands were analyzed separately, and all six position angles were used to determine the Faraday rotation measure. The six amplitudes were averaged together to produce the final mean polarized amplitude. For the vector plots shown below, the amplitudes were clipped to discard all values below three times the rms noise level of 0.2 mJy beam^{-1}, but for the fractional polarization determination all polarized intensities down to zero were included. Individual position angle uncertainties were typically 11°, although values with uncertainties up to 20° were included in the analysis.

A MOST image at a frequency of 843 MHz and a resolution of 45″ was kindly provided by A. Green for comparison purposes. The equipment and observing parameters for that image are given in the paper by Whiteoak & Green (1996).

3. RESULTS

3.1. *Total Intensity*

The full mosaicked total intensity image is shown in Figure 1*a*. The half-power beamwidth is 8″. As well as showing the SNR, this image illustrates some of the artifacts present in mosaic images with missing short spacings of the antennas. The most striking feature of this supernova remnant is the lack of any fine-scale features. It looks virtually identical to the MOST image, Figure 1*b* (Whiteoak & Green 1996), with a resolution of 45″. This is not an error in the data analysis, as point sources show the correct 8″ half-power width (compare Fig. 1*a* with 1*b*). Even the edge of the SNR is not sharp but very diffuse, as illustrated by the representative slices through the shell seen in Figure 2. The same effect is even seen in RCW 86 where the emission appears to come from bright extended patches, not the thin filaments seen in the optical-line images (Smith 1997).

Among the well-studied remnants, the radio morphology of G315.4−2.3 bears the most striking resemblance to Tycho (G120.1+1.4). Both shells consist of a set of arcs with radii often larger than the average radius of the periphery. In both, the arcs do not quite close at one location, leaving a noticable gap, and several of the arcs can be traced into the interior. G315.4−2.3 lacks, however, the sharp outer rims that delineate much of Tycho's silhouette (Dickel, van Breugel, & Strom 1991).

Also reminiscent of Tycho is that the general outline of the circular shell is similar in both the radio and the optical (Fig. 3). For the contour display of the radio emission, we have blanked some of the pixels right around the bright point source at $14^{h}41^{m}44^{s}.48$ and $-62°34'47''.1$, so as not to distract the viewer. The Hα filaments generally lie just outside the radio shell or just inside it. The latter placement could be caused by projection effects of filaments on the shell in front or back of the plane of the sky. Projection might also possibly explain the very notable lack of radio emission toward the sharp filaments on the west side of the remnant which are bright in Hα (Fig. 3) and look virtually identical in the X-ray band (Vink et al. 1997). These filaments appear to lie between about 0.65 and 0.85 of the radius of the remnant in that direction so that the projection of a thin shell along the line of sight would be less than half what it is at the edge. Such a reduction in brightness would make their detection marginal in the radio.

There is no good correlation of individual radio and optical features at any location in either position, orientation, or intensity. We note that the east rim has several spots that are nearly as bright as RCW 86 in the radio but less than 1/50 as bright in Hα. Toward RCW 86 itself, the brightest optical emission wraps around the western and southern sides of the brightest radio patch but lies inside the fainter outer radio feature on the southern edge (Fig. 4*a*), suggesting almost an inverse correlation. There is, however, a very faint Hα filament just at the outer edge of the radio emission in that direction. RCW 86 is conclusively shown to

[4] D. A. Green 1998, http://www.mrao.cam.ac.uk/surveys/snrs/.

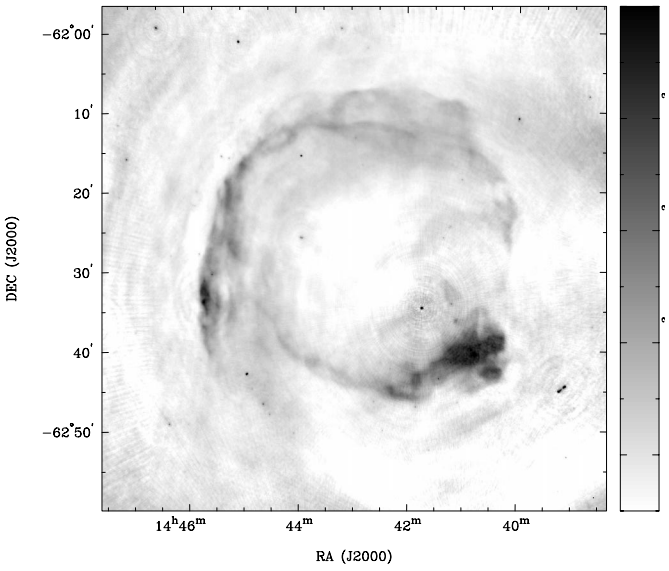

FIG. 1*a*

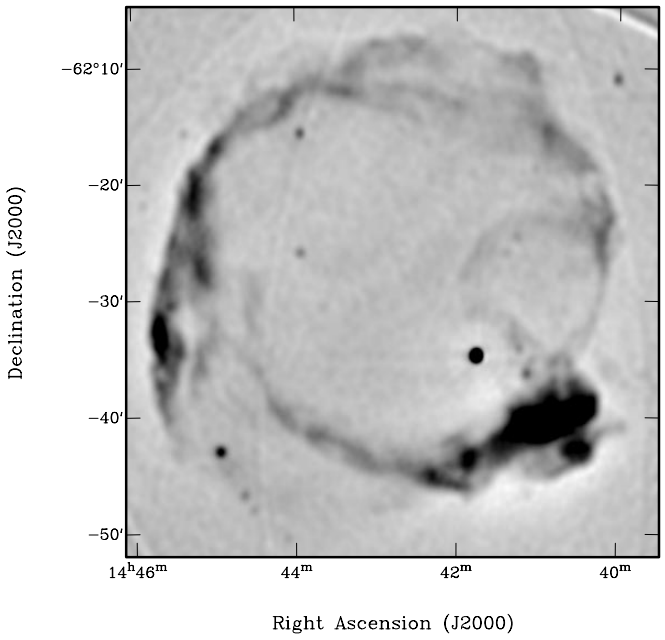

FIG. 1*b*

FIG. 1.—(*a*) Gray-scale image of the supernova remnant G315.4−2.3 and surroundings at a frequency of 1.34 GHz. The scale for the wedge is Jy beam^{-1}. The 8″ beam is shown as the tiny dot in the lower right corner of the plot. (*b*) A MOST image with a resolution of 45″ shown for comparison. The range of the gray scale is from 0 to 300 mJy beam^{-1}. Artifacts, including the 1°.2 grating ring, are discussed by Whiteoak & Green (1996).

be in radiative equilibrium from the [S II]/Hα ratio near 1.0 (from the images by Smith 1997).

In the north, both the radio and hard X-ray emission (Vink et al. 1997) extend well beyond the optical in several spots. The optical filament at $14^h43^m40^s$ and $-62°08'$ is particularly puzzling. It is bright in [S II] as well as Hα and is presumably shocked material in radiative equilibrium, but it appears to be sharply broken at the ends and sits outside a hole of the same length in the main northern shell. A radio slice through the region (Fig. 2*c*), on the other hand, shows that the radio emission just decreases continuously from the break in the optical shell out to the position of the apparently broken-off outer piece. The radio emission then appears to curve off toward the east and form a bubble, which returns to the brighter main shell at about $14^h44^m30^s$ and $-62°13'$. Perhaps the expanding material has hit a small hole in the interstellar medium.

In general, soft X-rays seem to follow the optical emission in both the radiative and nonradiative filaments, but the harder X-rays are different. The hard/soft X-ray ratio is generally high in the regions of significant radio emission, but there is certainly not a one-to-one correlation of features. The general configuration was interpreted by Vink et al. (1997) to mean that the hard emission represents a nonthermal power-law tail to the X-ray distribution.

3.2. *Polarized Emission*

The polarized emission is too faint to be reliably detected in most places but can be measured toward RCW 86 and at a few spots on the eastern rim of the SNR. The mean fractional polarization within the 2 mJy beam^{-1} total intensity contour toward RCW 86 is 8% with only small variations. The brightest feature on the east limb of G315.4−2.3 at $\alpha = 14^h46^m30^s$ and $\delta = -62°33'$, which has about the same total intensity as RCW 86, shows no polarization to less than 3%. It is only in a few regions farther to the north that any reliable polarization can be measured. In the most polarized patch at $14^h45^m05^s$ and $-62°21'$, the polarized fraction reaches about 15%. The regions of highest polarized intensity are indeed the same ones found at 2.7 and 5 GHz with resolutions of 8.′4 and 4.′4, respectively, by Milne & Dickel (1974, 1975). We note that the degree of polarization is low where the emission of RCW 86 is brightest and also where the X-ray emission is most intense. This is consistent with depolarization caused by differential Faraday rotation in the high-density gas present in those regions.

It is only in the brightest polarized regions that the position angles of the electric vectors can be measured with sufficient reliability within the 32 MHz bands to provide an accurate evaluation of the Faraday rotation. Using these data we have determined the Faraday rotation and thence, by rotation back to zero wavelength, the intrinsic direction of the *magnetic* field. These results are shown in Figure 5 along with the fractional polarization. In order to make them visible, the magnetic vectors and boxes representing the magnitudes of the Faraday rotation are plotted at only every tenth pixel for a separation of 2.5 beamwidths. This means that every vector is completely independent.

The Faraday rotation has a reasonably small range between +20 and +120 rad m^{-2} with most values near +70 rad m^{-2}. Typical uncertainties are around ±20 rad m^{-2}. This uncertainty can cause a significant error (about 50°) when rotated back to the intrinsic value at zero wavelength, but the consistency of the adjacent, but independently measured, vectors would suggest that they appear to be better determined than their formal errors would indicate. In the discussion we shall consider the position angles to be as shown.

4. DISCUSSION

There are several features of G315.4−2.3 that make it

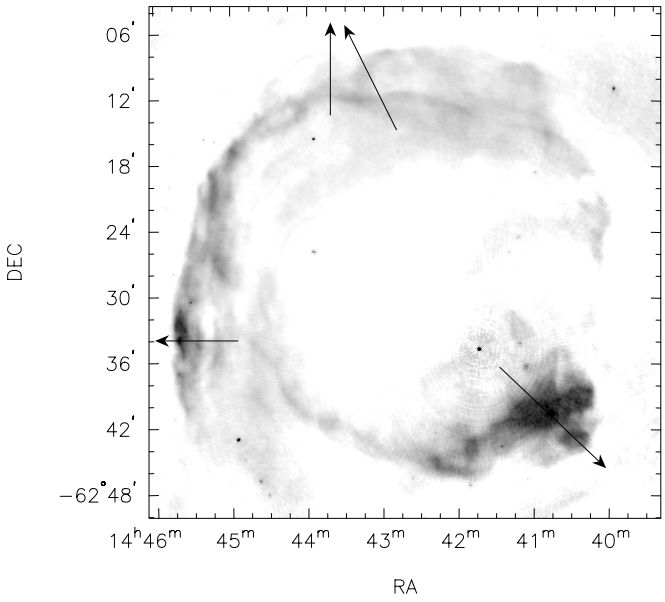

FIG. 2*a*

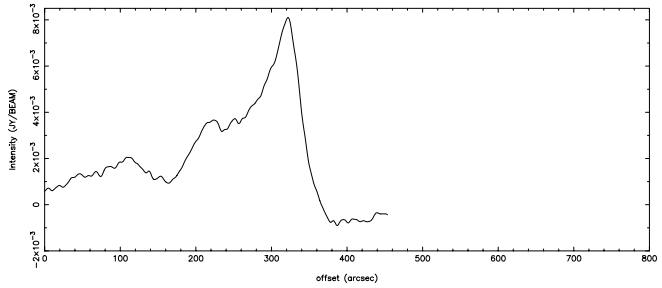

FIG. 2*b*

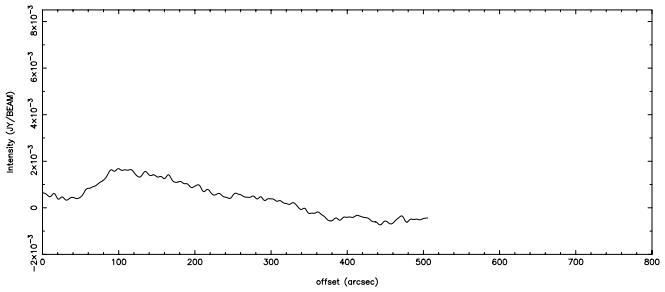

FIG. 2*c*

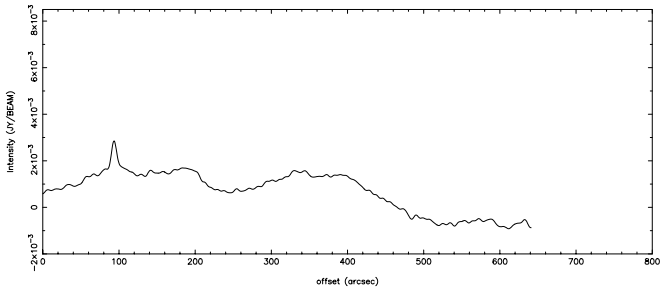

FIG. 2*d*

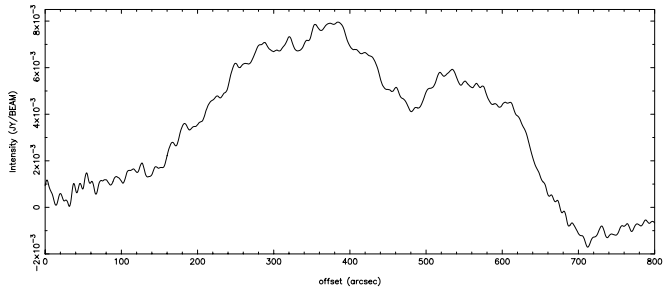

FIG. 2*e*

FIG. 2.—Sample slices through the (*a*) radio image of G315.4−2.3: (*b*) through the eastern rim; (*c*) through the northern "breakout" region; (*d*) through the northern rim and including a faint point source; and (*e*) through the region of RCW 86 itself. All the plots are to an identical scale.

very reminiscent of young remnants like Tycho's SNR and SNR 0519−690 in the LMC. We see thin, Balmer-dominated filaments outside a rather smooth radio shell with little fine structure. The filaments are still expanding with a rather high velocity of 600 km s^{-1} as measured by the widths of the broad component of the Balmer lines (Long & Blair 1990). The shell is reasonably complete and circular, although gaps and irregularities are beginning to appear. The magnetic field is radially oriented, and the radio spectral index of -0.61 ± 0.01 (Reynolds & Ellison 1992) is somewhat steeper than the average for SNRs. A steeper spectrum is characteristic of young shell SNRs (Dickel 1991).

The presence of forbidden-line emission, primarily in the nebulosity RCW 86, may seem to run counter to the "youthful" features just mentioned. However RCW 86 is somewhat reminiscent of the forbidden-line "fan" seen in the young SNR Kepler (SN 1604; van den Bergh, Marscher, & Terzian 1973). Even their shapes are similar, and practically the same spectral lines of [S II], [O II], [O III], [N II], etc., are seen in both (Leibowitz & Danziger 1983). Such features are also associated with substantial shock-heated dust, as shown by strong infrared emission (Greidanus & Strom 1990; Braun 1987). The proper motions of their filaments are low, less than 0.″02 yr^{-1} or less than 260 km s^{-1} for RCW 86 at the farther distance of 2.8 kpc (van den

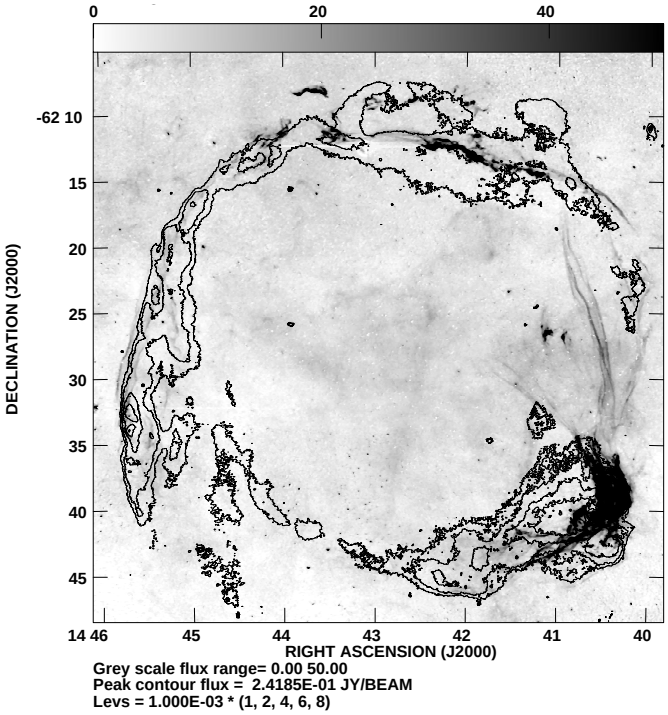

FIG. 3.—Hα gray scale (Smith 1997) and selected 1.34 GHz radio contours of the supernova remnant G315.4−2.3.

Bergh & Kamper 1977; Kamper, van den Bergh, & Westerlund 1995); this low a velocity has usually been interpreted in terms of swept-up circumstellar material. The one striking difference is the enhanced X-ray emission around RCW 86.

The nonradiative Balmer line emission, with both narrow and broad spectral components, is a common feature of young SNRs (Smith et al. 1991), though it can also be found in much older objects like the Cygnus Loop (Raymond et al. 1983), where, however, radiative forbidden-line emission dominates. From the spectral properties of the Balmer components, it is possible to derive a shock velocity, though this is somewhat dependent upon the degree of equilibration (Chevalier et al. 1980). We note that the width of the broad component in the generally accepted historical shell remnants (Tycho, Kepler, and SN 1006) ranges from 1500 to 2300 km s^{-1} (Chevalier et al. 1980; Smith et al. 1991), while in the Cygnus Loop a value of about 130 km s^{-1} is found (Hester, Raymond, & Blair 1994; Raymond et al. 1983). For G315.4−2.3, an FWHM of 660 km s^{-1} is observed (Long & Blair 1990). Since the three historical remnants range in age from 400 to 1000 yr, while the Cygnus Loop is usually reckoned to be $\simeq$104 years old (Blair et al. 1999), the intermediate velocity width in G315.4−2.3 suggests an intermediate age of several thousand years. On the low side, this could still be consistent with a supernova as recently as 1800 years ago.

A number of the age indicators mentioned above represent an evolutionary rather than physical age. Arguments for a young physical age center on the fact that there may have been a supernova in about the correct location in A.D. 185 (Clark & Stephenson 1977; but see Schaefer 1995) and a relatively close distance of about 1 kpc based on extinction measurements (Strom 1994). The latter allows the remnant to have a radius of about 6.5 pc, so it can have expanded at a reasonable rate for 1800 years. Alternatively, using optical spectroscopy of RCW 86 itself, Rosado et al. (1996) found a mean radial velocity of −33.2 km s^{-1}, which corresponds to a distance of 2.8 kpc for the Brand & Blitz (1993) model

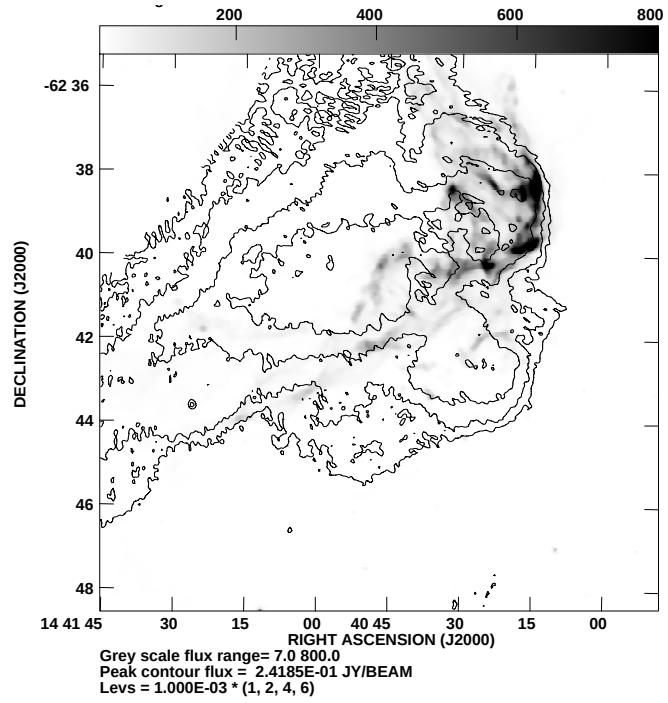

FIG. 4*a*

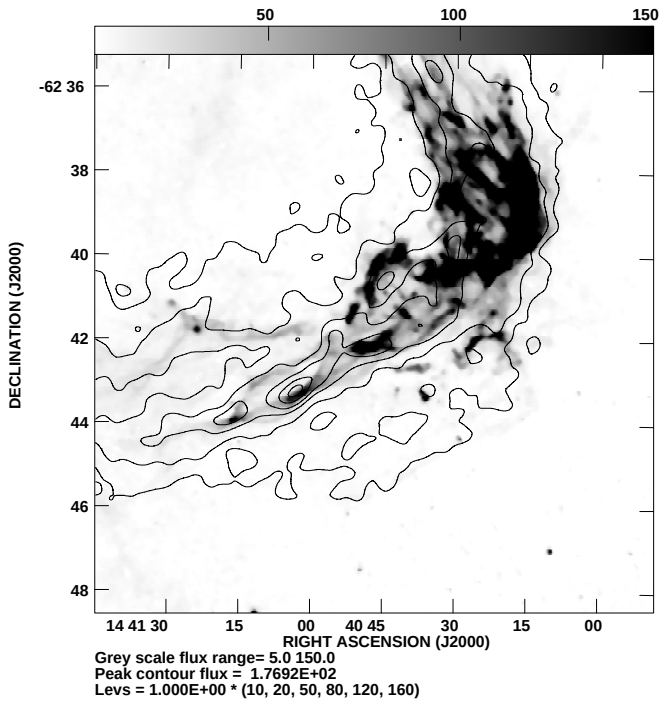

FIG. 4*b*

FIG. 4.—Region of RCW 86. (*a*) A logarithmic Hα gray-scale image in an attempt to show both the faint and bright emission with superimposed selected radio contours. For the contour display, the radio data have been blanked within 4′ of the bright point source, which would lie just at the top of the wedge on the northeastern edge of the image. (*b*) A linear Hα gray scale over a limited range with selected X-ray contours from the public *ROSAT* HRI image.

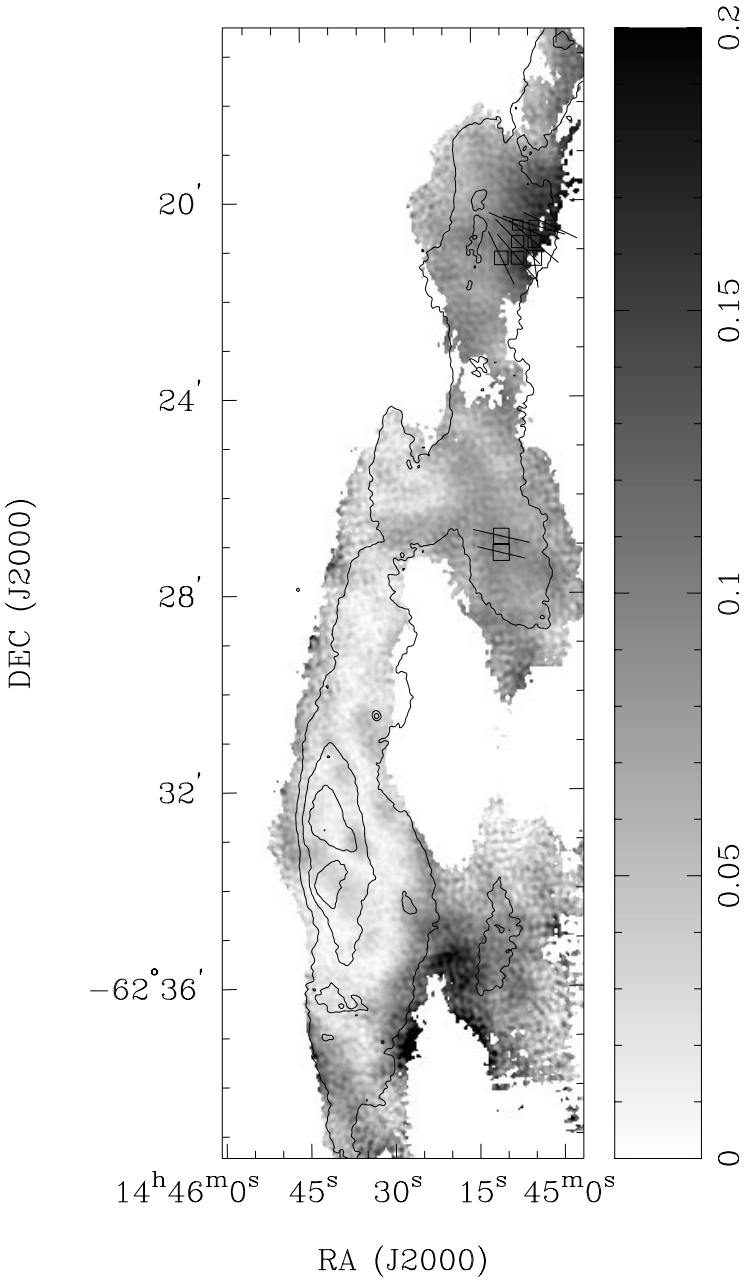

FIG. 5*a*

FIG. 5.—Radio polarimetric data on G315.4 − 2.3 at 1.34 GHz. The contours are the total intensity with values of 2, 4, and 6 mJy beam^{-1}. The gray scale is the fractional polarization with the ranges indicated on the wedges. The boxes indicate the Faraday rotation measure. The vectors show the direction of the *magnetic* field with the length proportional to the polarized intensity. (*a*) The east rim of the SNR. Only a few faint boxes and vectors are present near the northern end and two toward the center of the plot. A box diameter of 10″ represents a rotation measure of 38 rad m^{-2}, and a vector length of 10″ is a polarized flux density of 0.23 mJy beam^{-1}. (*b*) The RCW 86 region. A box diameter of 10″ represents a rotation measure of 58 rad m^{-2}, and a vector length of 10″ is a polarized flux density of 0.57 mJy beam^{-1}.

of galactic rotation. At this distance, G315.4−2.3 has a radius of about 18 pc. Expansion to this size in 1800 years implies a mean velocity of 10,000 km s^{-1}. Such a speed could be possible if the remnant were expanding inside an empty cavity and is just now encountering the inner walls. There is a small amount of shock-heated dust in the shell near RCW 86, less than 10^{-3} $M_{\odot}$ (Greidanus & Strom 1990) and a ridge of infrared emission along the eastern edge of the SNR (Arendt 1989; Greidanus & Strom 1990), which could be from dust in a cavity wall. The outer walls could still be neutral to give rise to the Balmer-dominated filaments. Although the size of the bubble would be too large to have been produced by the wind of a single progenitor star, Westerlund (1969) has identified an association of O stars surrounding the position of G315.4−2.3 at a distance of about 2.4 kpc. The supernova could have occurred in a bubble formed by more than one contributor.

An argument in favor of the larger, kinematic distance comes from mass estimates. For an expanding Type Ia remnant to have slowed down to 600 km s^{-1} (Long & Blair

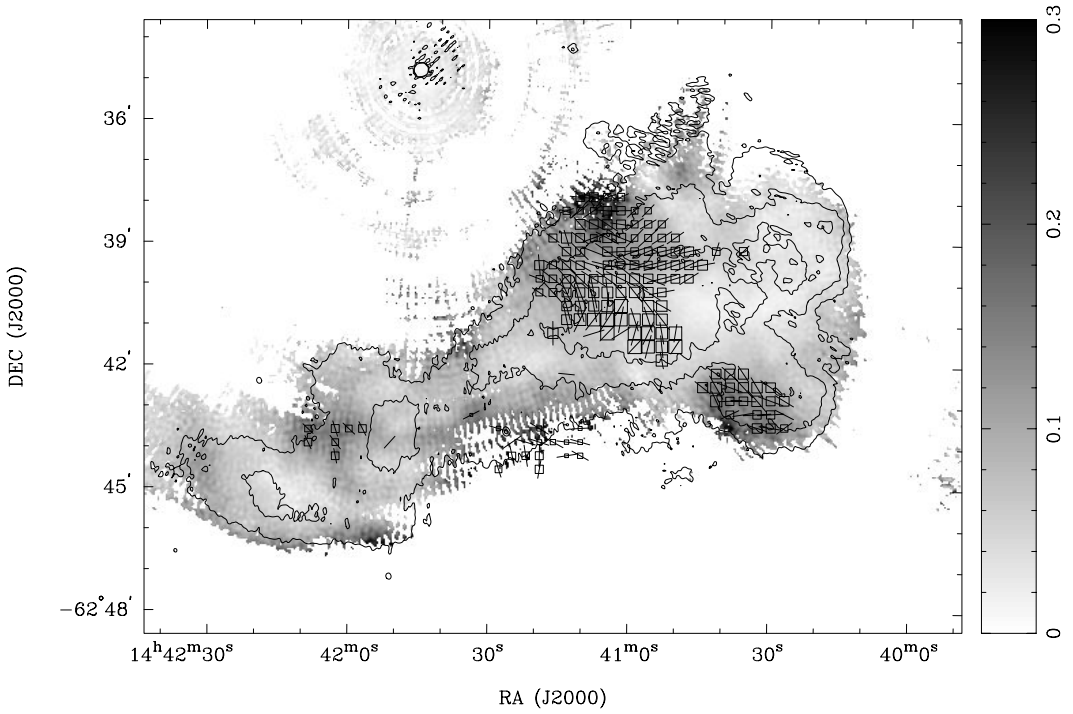

FIG. 5*b*

1990) from the canonical 10,000 km s^{-1}, it must have swept up about 200 times the ejected mass. Even if it was a Type II supernova with greater ejected mass and slower initial velocity, the total mass in the SNR must be on the order of 100 $M_{\odot}$.

The mass can be determined from the mean density and volume of the SNR. A number of workers using different techniques from different wavelength data but a common distance of 1 kpc have arrived at similar estimates for the density of the material in G315.4−2.3. From an *ASCA* pointing covering about $\frac{1}{5}$ of the remnant on the northeast side, Vink et al. (1997) found a mean initial density of about 0.2 cm^{-3} and 1–10 cm^{-3} toward RCW 86 in the southwest. Claas et al. (1989) found 0.11 cm^{-3} on the northeast side and 1.1 cm^{-3} toward the southwest from their *EXOSAT* data. Greidanus & Strom (1990) used *IRAS* infrared data to get a density of 0.6 cm^{-3}, weighted toward the region around RCW 86. Smith (1997) has found 0.9 cm^{-3} toward the Balmer filaments inside the western edge just north of RCW 86. These densities are all relatively low and support the idea of a bubble environment and interaction with a higher density clump on the southwest. The difference between northeast and southwest is also consistent with a density ratio of $\simeq 4$ found from theoretical modeling of G315.4−2.3 by Petruk (1999).

For convenience, we shall assume that $\frac{4}{5}$ of the remnant has a mean density of 0.2 cm^{-3} and $\frac{1}{5}$ has 1 cm^{-3}. At 1 kpc the mean radius is 6.5 pc, and the total volume is 3.4×10^{58} cm^3. The total mass is then 6.4 $M_{\odot}$, well below the necessary amount to slow the expansion to its present speed. If the SNR is at 2.8 kpc, however, the densities, which were determined from the emission measures, decrease by only the square root of the distance, whereas the volume increases as the cube of the distance. The resultant mass of 84 $M_{\odot}$ is certainly within a factor of 2 of what is required. Although this argument does place the SNR near 2.8 kpc, it does not distinguish between a massive progenitor or a low-mass one which just happened to occur in the vicinity of the association.

At the position of RCW 86, the expansion appears to have encountered a dense clump of material with sufficiently high density for radiative equilibrium in the filaments which show a ratio of the bright sulfur doublet at 671.7 and 673.1 nm to Hα of about 1.0 (Smith 1997). Radiative filaments generally show a nearly perfect one-to-one correspondence between images at radio and optical wavelengths, e.g., IC 443 (Mufson et al. 1986), but in RCW 86 we see that the bulk of the radio emission has no filamentary structure and lies inside the optical filaments. The smaller and somewhat fainter radio clump on the outside of RCW 86 toward the south is apparently featureless (Fig. 3), but looking at the very lowest levels, one sees that a plateau of faint optical nebulosity actually matches the radio extension quite well (Fig. 4*a*). The X-ray emission appears strongest between the optical filaments (Fig. 4*b*), which could be explained by just-shocked hot gas which has not yet cooled to radiative equilibrium. There is possibly some hardening in the X-ray emission where the radio emission is brighter (Vink et al. 1997). The shock may not yet have penetrated all of the dense cloud, and on the inner side, bright radio and X-ray emission may be enhanced by a reverse shock going back into the ejecta or previously swept-up material. The interaction should not extend to outside the dense feature, however, and we have no explanation for the peculiar outer radio clump.

The polarization structure observed on this fine scale is similar to that found by Dickel & Milne (1976) with a resolution of 8′.4. The most highly polarized regions seen with that resolution are also the brightest in the current study, and there is no particular correlation of polarized intensity and total intensity. Because of the greater brightness sensitivity afforded by the lower angular resolution observations, Dickel and Milne were able to measure the polarization over the entire SNR and find a nearly radial

pattern all around the shell. Where measured with the higher resolution on the eastern rim, the new data confirm that pattern of a radially oriented magnetic field with regard to the center of the SNR. Toward RCW 86, it starts in a radial direction, but as it approaches the brightest optical part of the nebula, the field appears to curve off as if it may be wrapping around the densest part of the cloud. This appears to be an example of how irregularities in the interstellar medium can affect the magnetic fields.

A mean Faraday rotation of $\simeq +60$ rad m^{-2} is found over most of the remnant. The one significant discrepancy in rotation measure between the current study and that of Dickel & Milne (1976) is just on the eastern side of RCW 86, where they found a value of about -150 rad m^{-2}. Perhaps in this complex area, convolution over different scale sizes can create a different rotation. Looking at other polarized background sources, we find the RM for two near the southwest corner: the brightest source that is seen through the remnant has RM $= +182$ rad m^{-2}, while another one (an extended double) about 12′ to the west of RCW 86 shows values in the range $+25$ to $+55$ rad m^{-2}. These values are consistent with the positive values found for the SNR emission. In their compendium of rotation measures, Simard-Normandin, Kronberg, & Button (1981) list nearby sources with both positive and negative values, although the tendency appears to be negative. This agrees with nearby (within 10°) pulsars, three of which have negative values with a mean of RM $= -12$ rad m^{-2}, while one (PSR J1428−55) has RM $= +4$ rad m^{-2}. On the basis of such measurements, Rand & Lyne (1994) have modeled the interstellar magnetic field and conclude that, in the general direction of G315.4−2.3, the field points away from the solar system (producing negative RM values). The presence of a Galactic object with RM > 0 runs counter to their conclusion, suggesting that in the direction of $l = 315°$ the field must have a more complex structure.

5. CONCLUSIONS

Although G315.4−2.3 has elements indicative of both youth and age, all of its major characteristics (nearly circular, limb-brightened outer shell, radially directed magnetic field, spectral index, thin, Balmer-dominated filaments, no detailed correlation between radio and optical emission) are most frequently seen in young-shell SNRs. The radio morphology is most similar to that of 3C 10 (Tycho), except for the sharp, narrow outer rims which delineate most of the younger remnant's periphery (Dickel et al. 1991); there is no trace of such a component in MSH 14−*63*. It may be significant, however, that the outer rim is not seen along the eastern edge of 3C 10, where there is evidence of much interaction with the ambient medium. Perhaps this component, which coincides with the X-ray edge (and hence the outer blast wave), is a transient phenomenon that disappears as the blast wave becomes fully adiabatic. We also note that 3C 10 is unique in showing this distinct outer rim.

RCW 86, the high-density southwestern corner of MSH 14−*63*, remains the most puzzling feature in the remnant and is perhaps the key to what is going on. The obvious explanation, that the blast wave has encountered a high-density cloud, is difficult to rhyme with the fact that part of this emission extends beyond the average radius of the nearly circular shell. An encounter with a dense cloud should lead to a concave dent in the shell, not to a convex blister. A completely different possibility is that RCW 86 is where a compact clump of the exploded star is strongly interacting with the interstellar matter. The boomerang appearance of the X-ray emission here (Fig. 4) strikingly resembles an outward-moving Mach cone, and similar features have been identified in the Vela SNR (Aschenbach, Egger, & Trümper 1995; Strom et al. 1995). Such an encounter with a dense region would be by chance.

We thank Jacco Vink for help with the X-ray data, R. Chris Smith for providing the optical data, Anne Green for help with the MOST data, and all three for valuable discussions. Tom Brink assisted with some of the early data analysis. The thoughtful report by the referee, David Green, is greatly appreciated. J. R. D. gratefully acknowledges a Visitor's Fellowship from the Netherlands Foundation for Scientific Research (NWO) during his very enjoyable stay at ASTRON.

REFERENCES

Arendt, R. G. 1989, ApJS, 70, 181
Aschenbach, B., Egger, R., & Trümper, J. 1995, Nature, 373, 587
Australia Telescope. 1992, J. Electrical Electron. Eng. Australia, 12, 2
Blair, W. P., Sankrit, R., Raymond, J. C., & Long, K. S. 1999, AJ, 118, 942
Brand, J., & Blitz, L. 1993, A&A, 275, 67
Braun, R. 1987, A&A, 171, 233
Caswell, J. L., Clark, D. H., & Crawford, D. F. 1975, Australian J. Phys. Astrophys. Suppl., 37, 39
Chevalier, R. A., Kirshner, R. P., & Raymond, J. C. 1980, ApJ, 235, 186
Chin, Y.-N., & Huang, Y.-L. 1994, Nature, 371, 398
Claas, J. J., Smith, A., Kaastra, J. S., de Korte, P. A. J., & Peacock, A. 1989, ApJ, 337, 399
Clark, D. H., & Stephenson, F. R. 1977, The Historical Supernovae (Oxford: Pergamon Press), 83
Dickel, J. 1991, in Supernovae, ed. S. Woosley (Santa Cruz: Summer Workshop), 675
Dickel, J. R., & Milne, D. K. 1976, Australian J. Phys., 29, 435
Dickel, J. R., van Breugel, W. J. M., & Strom, R. G. 1991, AJ, 101, 2151
Greidanus, H., & Strom, R. G. 1990, A&A, 240, 385
Hester, J. J., Raymond, J. C., & Blair, W. P. 1994, ApJ, 420, 721
Hill, E. R. 1967, Australian J. Phys., 20, 297
Kamper, K. W., van den Bergh, S., & Westerlund, B. 1995, BAAS, 186, 3705
Leibowitz, E. M., & Danziger, I. J. 1983, MNRAS, 204, 273
Long, K. S., & Blair, W. P. 1990, ApJ, 358, L13
Mills, B. Y., Slee, O. B., & Hill, E. R. 1961, Australian J. Phys., 14, 497
Milne, D. K., & Dickel, J. R. 1974, Australian J. Phys., 27, 549
Milne, D. K., & Dickel, J. R. 1975, Australian J. Phys., 28, 209
Mufson, S. L., McCollough, M. L., Dickel, J. R., Petre, R., White, R., & Chevalier, R. A. 1986, AJ, 92, 1349
Petruk, O. 1999, A&A, 346, 961
Pisarski, R. L., Helfand, D. J., & Kahn, S. M. 1984, ApJ, 277, 710
Rand, R. J., & Lyne, A. G. 1994, MNRAS, 268, 497
Raymond, J. C., Blair, W. P., Fesen, R. A., & Gull, T. R. 1983, ApJ, 275, 636
Reynolds, S. P., & Ellison, D. C. 1992, ApJ, 399, L75
Rodgers, A. W., Campbell, C. T., & Whiteoak, J. B. 1960, MNRAS, 121, 103
Rosado, M., Ambrocio-Cruz, P., LeCoarer, E., & Marcelin, M. 1996, A&A, 315, 243
Schaefer, B. E. 1995, AJ, 110, 1793
Simard-Normandin, M., Kronberg, P. P., & Button, S. 1981, ApJS, 45, 97
Smith, R. C. 1997, AJ, 114, 2664
Smith, R. C., Kirshner, R. P., Blair, W. P., & Winkler, P. F. 1991, ApJ, 375, 652
Strom, R. G. 1994, MNRAS, 268, L5
Strom, R. G., Johnston, H. M., Verbunt, F., & Aschenbach, B. 1995, Nature, 373, 590
van den Bergh, S., & Kamper, K. W. 1977, ApJ, 218, 617
van den Bergh, S., Marscher, A. P., & Terzian, Y. 1973, ApJS, 26, 19
Vink, J., Kaastra, J. S., & Bleeker, J. A. M. 1997, A&A, 328, 628
Westerlund, B. E. 1969, AJ, 74, 879
Westerlund, B. E., & Mathewson, D. S. 1966, MNRAS, 131, 371
Whiteoak, J. B. Z., & Green, A. J. 1996, A&AS, 118, 329